AIAA JOURNAL
Vol. 47, No. 12, December 2009

Control of High-Temperature Supersonic Impinging Jets Using Microjets

Rajan Kumar,* Sladana Lazic,† and Farrukh S. Alvi‡
Florida A&M University and Florida State University, Tallahassee, Florida 32310

DOI: 10.2514/1.39061

The flowfield associated with supersonic impinging jets has been of interest to both engineers and researchers for some time due to its wide range of practical applications and its complex nature from a fundamental fluid dynamic point of view. An example of supersonic impinging jets occurs in short takeoff and vertical landing aircraft, for which the highly oscillatory flowfield and the associated acoustic loads are also accompanied by a dramatic loss in lift during hover, severe ground erosion of the landing surface, and hot gas ingestion into the engine inlets. Another characteristic feature of this flowfield is an intensive heat transfer between the jet and the impingement surface. In the past we have examined impinging jets and their control using microjets at cold conditions; the present study is a step toward examining this flowfield and the effectiveness of microjet control at increasingly realistic thermal conditions. An ideally expanded, Mach 1.5 primary jet issuing from an axisymmetric nozzle was heated up to a stagnation temperature of ∼500 K. Mean and unsteady temperature and pressure measurements were obtained on a lift plate representative of the undersurface of an aircraft and on the ground plane over a range of nozzle-to-plate distances (representing aircraft hover conditions). In addition, near-field noise was also measured using a microphone. The velocity field of the impinging jet for both cold and hot conditions was mapped using particle image velocimetry. Our results show that the temperature recovery factor at the stagnation point on the ground plane is strongly dependent on the temperature ratio and nozzle-to-plate distance, similar to observations in subsonic impinging jets. The hover lift loss for hot jets is much higher than for cold jets, nearly 75% of the primary jet thrust at small nozzle-to-plate distances. The pressure fluctuations generated by hot impinging jets are also substantially higher than their cold counterparts. As in cold jets, pressure and noise spectra for hot jets show discrete, high-amplitude acoustic tones (generally known as impinging tones) at frequencies varying with jet temperature. The activation of microjet control shows a substantial reduction in pressure fluctuations both in terms of overall sound pressure levels (up to 20 dB on the ground plane and 15 dB on the lift plate) and the attenuation of discrete, high-amplitude impinging tones (up to 32 dB). High-temperature peaks were observed in the temperature spectra at frequencies corresponding to impingement tones in the pressure and noise spectra; these were also substantially attenuated with microjet control. As much as 50% of the lift loss was recovered by using control for hot jets at smaller nozzle-to-plate distances. In general, the results provide evidence of the feasibility of using this active control approach under increasingly realistic conditions to achieve desired reductions in noise, unsteady pressures, and thermal loads.

I. Introduction

MANY examples of flow impingement of a jet on a solid surface can be found in engineering applications, including the launch of a rocket, takeoff and landing of a short takeoff and vertical landing (STOVL) aircraft, thrust vector control of a solid rocket motor or an aircraft exhaust, turbine blade cooling, electronic equipment cooling, and paper drying. For an efficient design of such systems, it is important to understand the flowfield associated with impinging jets. In particular, STOVL aircraft during hover produce high-temperature impinging jets on the landing surface. These lift-producing jets result in a high-temperature, turbulent, and highly oscillatory flowfield. This leads to severe ground erosion of the landing surface, lift loss due to entrainment of high-speed flow near the nozzle exit, very high unsteady loads on the nearby structures, and hot gas ingestion into the engine inlets. High levels of overall sound pressure levels (OASPL) associated with high-temperature supersonic impinging jets are a cause of concern due to sonic fatigue failure of the aircraft structure and a major source of noise pollution for personnel in the aircraft vicinity.

The flowfield properties of a supersonic impinging jet have been investigated by many researchers in the past, including Donaldson and Snedeker [1], Lamont and Hunt [2], Powell [3], Tam and Ahuja [4], Messersmith [5], Alvi and Iyer [6], Krothapalli et al. [7], and more recently Henderson et al. [8]. These studies clearly demonstrated the unsteady behavior of impinging jets and the presence of high-amplitude discrete impinging tones. Krothapalli et al. [7] demonstrated that generation of large-scale structures in the jet shear layer induces high entrainment velocity near the nozzle exit and, in turn, significant lift loss during hover. It is now well known that the highly unsteady behavior of the impinging jets is due to a feedback loop between the flow and acoustic fields, which leads to the aforementioned adverse effects. The concept of the feedback loop and its understanding has its roots in the pioneering research of Powell [9], who explained the feedback loop associated with edge tones generated by high-speed jets. A number of the general features of the feedback loop associated with impinging tones are similar to that elucidated by Powell for edge tones. (It should, however, be noted that despite the overall similarities in terms of flow-acoustic resonance, there are differences in many of the details. As an example, the sound producing source mechanisms, a subject of considerable research, in the two flows may be different). In a similar manner, as noted by Tam and Ahuja [4] and detailed by Krothapalli et al. [7], the feedback loop in the impinging jet is initiated as instability waves in the shear layer of the jet at the nozzle lip. These instability waves grow in size into large-scale vortical

Presented as Paper 360 at the 46th AIAA Aerospace Sciences Meeting and Exhibit, Reno, NV, 7–10 January 2008; received 12 June 2008; revision received 28 July 2009; accepted for publication 29 July 2009.

*Research Scientist, Department of Mechanical Engineering. Member AIAA.
†Research Associate, Department of Mechanical Engineering.
‡Professor, Department of Mechanical Engineering, Florida Center for Advanced Aero-Propulsion, College of Engineering. Associate Fellow AIAA.

structures as the jet travels downstream. In the case of impinging jets, the ground plane acts as a physical obstruction similar to the "edges" in edge tones. Upon impingement, these vortices generate large pressure fluctuations, which in turn travel upstream in the ambient flow in the form of acoustic waves. Upon reaching the nozzle exit, these acoustic waves excite the shear layer and complete the feedback loop.

There have been many attempts to suppress the feedback loop generated by edge tones, screech tones, and impinging tones using both passive and active control methods. For example, Karamcheti et al. [10] suppressed edge tones by placing two plates perpendicular to the jet centerline. Kweon et al. [11] attenuated the screech tones and the broadband shock-associated noise over a range of nozzle pressure ratios by placing two thin wires orthogonally to the jet axis. Elavarasan et al. [12] attenuated the feedback loop by placing a circular plate near the nozzle exit, achieving a reduction in the near-field OASPL and reasonable lift recovery. Sheplak and Spina [13], with the help of high-speed coflow, shielded the primary jet from the acoustic field. Shih et al. [14] successfully suppressed screech tones of nonideally expanded jets using counterflow at the nozzle exit. All these techniques have shown reasonable reductions in noise levels but only over a limited range of geometric and flow parameters and with major modifications in the aircraft design required.

A recent approach to suppress the feedback mechanism of supersonic impinging jets using an array of high-momentum microjets appropriately placed near the nozzle exit has shown highly promising results [15–19]. This control-on-demand technique has many advantages over traditional passive and active control methods and has proven to be successful over a range of geometric and flow conditions. With the help of particle image velocimetry (PIV) measurements, Alvi et al. [19] have shown that one of the main mechanisms at work is the introduction of streamwise vorticity at the expense of azimuthal vorticity of the main jet. A reduction in the primary shear-layer instability, attenuation of upstream propagating acoustic waves, and disruption of spatial coherence between large-scale structures and the acoustic field lead to an overall attenuation in the feedback loop. These experiments have conclusively demonstrated the effect of microjet control in reducing the undesirable effects of impinging jets. In a related microjet control study, Alkislar et al. [20] recently demonstrated the effectiveness of microjet injection and the role of streamwise vortices for reducing the mixing noise in a subsonic freejet. However, these experiments have only been conducted at cold conditions. From an application point of view, it is very important to examine the effectiveness of high-momentum microjet-based control at high temperatures for impinging jets as well as freejets. Although the noise sources and the aeroacoustic properties are different in free and impinging jets, there are similarities in the vorticity generation mechanisms through the use of microjets (see Alkislar et al. [20] and Alvi et al. [19]). In this study, our focus is on the control of hot supersonic impinging jets.

The primary objective of the present study is to characterize the properties of high-temperature impinging jets and to examine the effectiveness of high-momentum microjet control under these conditions. An ideally expanded supersonic impinging jet issuing from an axisymmetric converging–diverging nozzle ($M = 1.5$) was heated up to a total temperature of 480 K. Temperature and pressure measurements were made on the lift plate and ground plane over a range of geometric and flow parameters. Near-field noise measurements were made using a microphone. Global flow features of an impinging jet and its control were qualitatively studied using shadowgraph flow visualizations at selected test conditions. The velocity field for both free and impinging jets was also measured using PIV at selected conditions. This paper provides a description of the experimental setup, details of measurements made, typical results, implications, and concluding remarks.

II. Experiments

A. Test Facilities and Models

The experiments were carried out at the STOVL supersonic jet facility of the Advanced Aero-Propulsion Laboratory (AAPL) located at Florida State University. This facility is mainly used to study jet-induced phenomena on STOVL aircraft during hover. It is capable of running single and multiple jets at design conditions up to $M = 2.2$. The ground plate is mounted on a hydraulic lift and can be moved up and down to simulate different distances from aircraft to ground plane. High-pressure compressed air ($\sim$160 bar) stored in large storage tanks (10 m^3) is used to drive the facility. More details of the facility can be found in Krothapalli et al. [7] and Alvi et al. [19].

A schematic of the test model and measurement apparatus used in the present experiments is shown in Fig. 1. The measurements were made on an ideally expanded jet issuing from a converging–diverging axisymmetric nozzle. The throat and exit diameters (d, d_e) of the nozzle are 2.54 and 2.75 cm, respectively. The diverging section of the nozzle is straight walled with a 3 deg divergence angle from the throat to the nozzle exit. The nozzle has a design Mach number of 1.5 and was operated at a nozzle pressure ratio (NPR = stagnation pressure/ambient pressure) of 3.7, corresponding to an ideally expanded jet. The air is heated using an inline flow heater up to a maximum stagnation temperature of

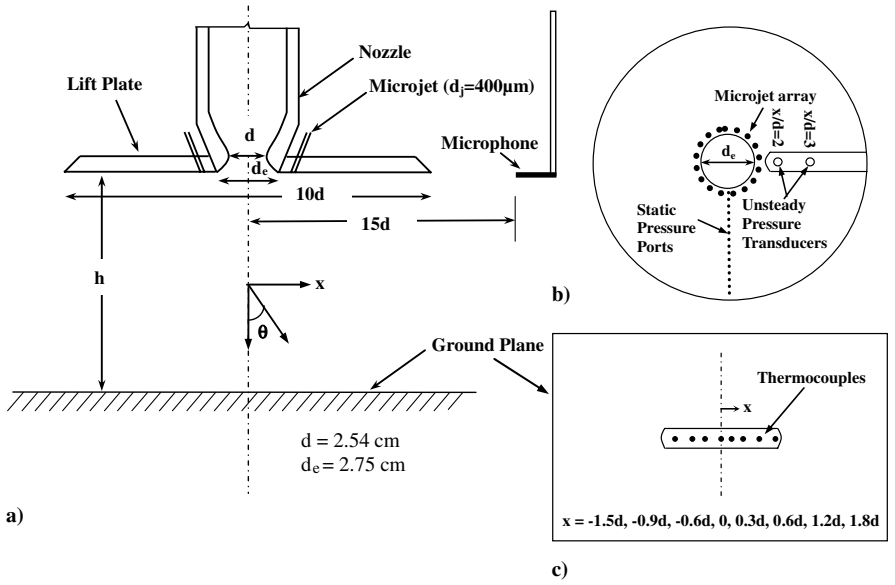

Fig. 1 Schematic of the experimental setup: a) overall arrangement; b) lift plate showing locations of microjets, static pressure ports, and unsteady pressure transducers; and c) ground plane showing locations of thermocouples.

480 K at the nozzle exit, resulting in a temperature ratio (TR= stagnation temperature/ambient temperature) of 1.6. A circular plate with a diameter of 25.4 cm ($10d$) was flush mounted with the nozzle exit. This plate, henceforth referred to as the lift plate, represents a generic aircraft platform and has a central hole equal to the nozzle exit diameter through which the jet is issued (Fig. 1b). An aluminum plate with the dimensions of $1\ \text{m} \times 1\ \text{m} \times 25$ mm represents the ground plane and is mounted on the hydraulic lift directly under the nozzle exit (Fig. 1c).

B. Measurements and Instrumentation

1. *Temperature, Pressure, and Near-Field Noise Measurements*

The temperature distribution on the ground plane and lift plate were measured using K-type thermocouples. The ground plane and lift plate were instrumented with eight and six thermocouples, respectively; the precise locations on the ground plate are given in Fig. 1. The flow-induced lift loss was estimated by measuring the mean static pressure distribution on the lift plate with 19 pressure ports along a radial line. The static pressures were measured by scanning each port with a Scanivalve™ connected to a $\pm$1-psid-range Validyne™ strain gauge pressure transducer. Unsteady pressure measurements on the ground plane and lift plate were obtained using high-frequency response, miniature (1.6-mm-diam) Kulite™ pressure transducers with a 100 psia and $\pm$5 psid range, respectively. The transducer on the ground plane was mounted at $x/d = 0$ (the stagnation point) and $x/d = 2$ (5.08 cm from the centerline of the jet) at all temperatures tested. The unsteady pressure field on the lift plate was measured using two transducers mounted at $x/d = 2$ and 3 from the nozzle centerline.

In addition to temperature and pressure measurements, near-field acoustic measurements were made using a 0.635-cm-diam (1/4-in.-diam) Brüel & Kjær microphone placed at $x/d = 15$ from the nozzle centerline and 90 deg with respect to the jet axis (Fig. 1a). All sensors (thermocouples, pressure transducers, and the microphone) were carefully calibrated before each set of experiments. To minimize sound reflections during these measurements, parts of the rig and nearby metal surfaces were covered with acoustic foam. The temperature, pressure, and acoustic signals were acquired through high-speed National Instruments digital data acquisition cards using Labview™ and were processed offline. The transducer signals were conditioned using Stanford™ filters (model SR650) and simultaneously sampled at 70 kHz. Standard fast Fourier transform (FFT) analysis was used to obtain spectra and OASPL from these measurements. A total of 100 FFTs of 4096 samples each were averaged to obtain a statistically reliable estimate of the narrowband spectra.

2. *Velocity Measurements Using Particle Image Velocimetry*

The velocity field data at the central plane were obtained using PIV. Details of the PIV technique and associated hardware used in the present experiments are similar to Krothapalli et al. [7] and Alvi et al. [19]. Briefly, a double-pulsed Nd.YAG laser from Spectra-Physics with a maximum beam intensity of $\sim$400 mJ/pulse was used for illumination of the flowfield. A light sheet with a thickness of about 1 mm was created using a combination of spherical and cylindrical lenses. A schematic of the experimental and optical arrangement in the planar PIV are shown in Fig. 2. The primary cold jet was seeded using very small ($\approx$0.3 μm) Rosco fog™ fluid droplets generated using a modified Wright Nebulizer (Krothapalli et al. [7]). At high temperatures (>450 K), these fog fluid droplets turned into smoke and therefore added the challenge of seeding the flow for high-temperature impinging jets. This was overcome by using extra-virgin olive oil (smoke point $\approx$480 K) to generate the seed particles. The ambient air was seeded with smoke particles (1–5 μm) produced by a Rosco 1600 fog generator. The PIV images were acquired at a rate of 15 Hz using a charge-coupled device (CCD) camera (Kodak ES1.0) with a resolution of $1008(H) \times 1018(V)$ pixels, where each pixel size is $9 \times 9\ \mu\text{m}^2$. The camera was positioned at 90 deg to the jet axis. The pulse separation between the two laser pulses was kept at 1–1.2 μs. An image-matching approach for digital processing, similar to that used in previous experiments at AAPL (Krothapalli et al. [7] and Alvi et al. [19]), was used to extract particle displacement and the velocity field. In this processing scheme, the interrogation window is defined by the particle images, ranging from 3 to 4 pixels^2. The flowfield at every point is calculated using a least-squares fitting algorithm based on a second-order polynomial. This technique results in a second-order accuracy in calculating the flowfield at each point in the flow. The details of this technique are available in Lourenco and Krothapalli [21].

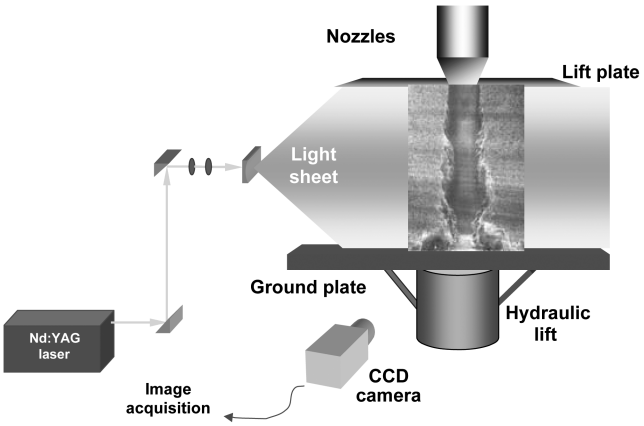

Fig. 2 Schematic of the experimental and optical arrangement of the planer PIV.

3. *Flow Visualization*

Flow visualizations were obtained using a conventional mirror-based, single-pass shadowgraph method. A white-light Xenon pulsed flash lamp with a 5–10 μs pulse duration was used as the light source. Two 31.75-cm-diam (12-in.-diam) first surface spherical mirrors with a focal length of 254 cm were mounted on the either side of the jet. A Kodak Megaplus ES1.0 digital camera, similar to the one used for PIV, was used for image acquisition. This method of flow visualization was only used for the cold jet (temperature ratio (TR) = 1.0). At higher temperatures, the heating of the ambient air makes the image noisy due to thermal currents.

C. Measurement Uncertainties

The thermocouples and pressure transducers were carefully calibrated before the tests, and appropriate calibration constants were used to calculate the temperatures and pressures. Based on repeatability, instrument precision, and errors introduced due to digitization and other sources, the overall uncertainties in the temperature and the mean static pressure are $\pm$2 K and $\pm$0.002 psi, respectively. The unsteady pressures on the lift plate and ground plane were measured using $\pm$5 psid and 100 psia Kulite pressure transducers, respectively. Uncertainty analysis show that the rms values of the unsteady lift plate and ground plane pressures were measured with an overall uncertainty of $\pm$0.02 and $\pm$0.2 psi, respectively, and that the uncertainty associated with the microphone OASPL was $\pm$0.5 dB.

The uncertainties in the velocity measurements are mainly due to errors in the measurement of particle displacement, particle lag, and the number of samples used for averaging the mean and turbulent quantities. In spite of the fact that we used very small particles ($\approx$0.3 μm), some particle lag always occurs, mainly in the region of high-velocity gradients such as shear layers and shock waves. In the present experiments, a large number of pairs (1000 pairs) were sampled to minimize sampling inaccuracies. Because the velocity field is not known a priori, there is no basis for an absolute comparison of the measured flowfield to a "known" flow. The mean velocity measurements at the jet exit were found to be within 1% of the velocities predicted from 1-D gas dynamics for both cold and hot jets. This 1% uncertainty covers the variance between measurements at the same nominal conditions.

Table 1 Test matrix

Serial no.	Type of measurement	NPR	TR	Nozzle to plane distance, h/d	Measurement locations
1	Temperature	3.7	1.0, 1.2, 1.4, 1.6	2–12	Ground plane $x/d = -1.5$–1.8 (eight thermocouples) Lift plate $x/d = 1.5$–4 (six thermocouples)
2	Static pressure	3.7	1.0, 1.2, 1.4, 1.6	1.5–10	Lift plate $x/d = 1.5$–10 (19 pressure ports)
3	Unsteady pressure	3.7	1.0, 1.2, 1.4, 1.6	2–12	Ground plane $x/d = 0$, 2 (two Kulites) Lift plate $x/d = 2$, 3 (two Kulites)
4	Near-field noise	3.7	1.0, 1.2, 1.4, 1.6	2–12	Microphone at $x/d = 15$
5	Shadowgraph flow visualization	3.7	1.0	4	——
6	PIV	3.7	1.0, 1.4	5, freejet	——

D. Test Conditions

The experiments were conducted at a nozzle pressure ratio (NPR) of 3.7, which corresponds to a nominally ideally expanded Mach 1.5 jet flow. The jet stagnation temperature was varied from 300 to 480 K, corresponding to a TR of 1.0–1.6, and was controlled within ± 2 K. The test Reynolds number based on exit velocity and nozzle diameter of the cold jet was 7×10^5. The distance from the nozzle to the ground plane, h, varied from 2 to $12d$. All tests conducted during this experiment are summarized in Table 1, but only a few representative results are discussed in this paper.

A total of 16 microjets were flush mounted circumferentially on the lift plate around the main jet to implement active flow control. A schematic of the mounting arrangement is shown in Fig. 1. The jets issued from 400-μm-diam stainless steel tubes mounted at an inclination of 60 deg with respect to the main jet axis. The supply for the microjets was provided from compressed nitrogen cylinder through a plenum chamber. The microjets were operated at a pressure of 100 psia, and the combined mass flux from all the microjets was less than 0.5% of the primary jet mass flux for all cases examined in this study.

III. Results and Discussion

The focus of the present study is to characterize the properties of hot impinging jets and examine the effectiveness of high-momentum microjet-based control for hot jets. Limited flow visualization results at selected test conditions will be presented to illustrate overall/global flow features associated with the impinging flow. The velocity field is examined using PIV measurements. Results of temperature distributions on the ground plane are followed by static pressure measurements to estimate lift loss during hover. The flowfield associated with hot impinging jets is characterized with unsteady temperature and pressure data and near-field acoustic characteristics.

A. Flow Visualization

A conventional shadowgraph technique was used to visualize the global flow features associated with the impinging jet flow and its control using microjets. Instantaneous shadowgraph images at TR $= 1.0$ and $h/d = 4$ without and with control are shown in Figs. 3a and 3b, respectively. It may be observed that the impinging jet flowfield (Fig. 3a) consists of large-scale, azimuthal, vertical structures in the jet shear layer along with multiple strong acoustic waves traveling up and down. These impinging and reflecting acoustic waves are the source of high-amplitude impingement tones observed in the pressure spectra shown subsequently (see Fig. 12). The presence of strong vortices in the jet shear layer explains the temperature recovery and lift-loss behavior of impinging jets, which will be discussed in Sec. III.C. With the activation of microjets (Fig. 3b), the flow features are significantly different. First of all, the strength of the large-scale azimuthal vortices in the shear layer has been significantly reduced so that they are barely visible in the shadowgraph image. The strong acoustic waves, clearly seen in Fig. 3a, have now been completely eliminated with the activation of control (Fig. 3b). A close and careful examination of the image in Fig. 3b reveals the existence of streamwise streaks in the primary jet, which suggest the presence of streamwise vortices due to microjets. These qualitative measurements are very much in line with the quantitative results, which will be discussed in the next few paragraphs. Unfortunately, this technique could not be used for hot jets because the thermal currents created by the hot ambient air made such visualizations unclear.

B. Temperature Distributions on the Impingement Plane

The measured temperatures are expressed in an often-used dimensionless form as the temperature recovery factor r. It is defined as

$$r = 1 + \frac{(T - T_0)}{T_d} \tag{1}$$

where T is the wall temperature, T_0 is the stagnation temperature of the jet, and T_d is the dynamic temperature of the jet. The value of T_d in Eq. (1) is estimated using the following relation (Goldstein et al. [22]):

$$T_d = \frac{U_j^2}{2C_P} = \frac{[(\gamma - 1)/2]M^2}{1 + [(\gamma - 1)/2]M^2} T_0 \tag{2}$$

Figure 4 shows the stagnation temperature recovery factor r_0 at the stagnation point ($x = 0$ on the ground plane; see Fig. 1c) as a function

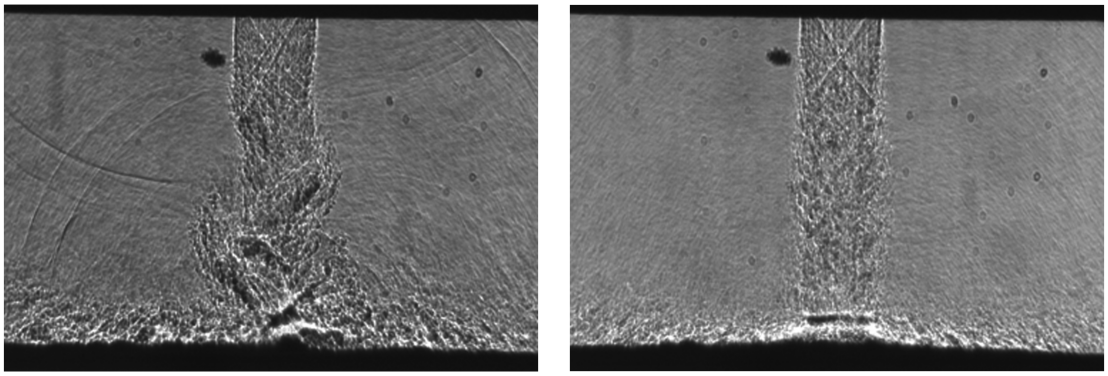

a) No control b) With control

Fig. 3 Instantaneous shadowgraph images at TR $= 1.0$ and $h/d = 4$.

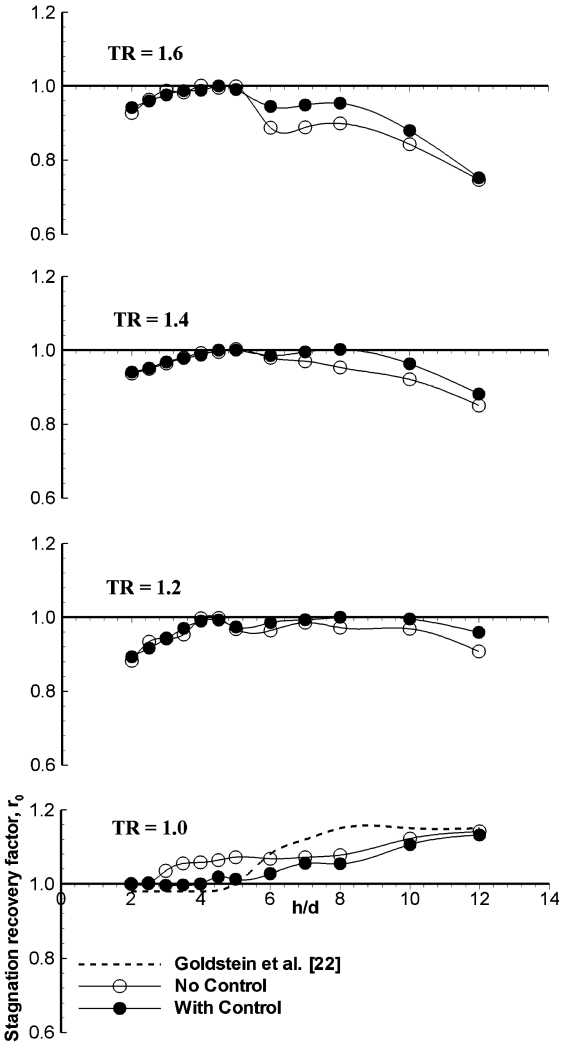

Fig. 4 Effect of temperature ratio on the stagnation temperature recovery factor.

of h/d at various temperature ratios, with and without microjet control. The temperature recovery factor at the stagnation point for a subsonic impinging jet from Goldstein et al. [22] has also been shown here for comparison; Goldstein's data correspond to a cold jet at $M = 0.47$ and $Re = 1.24 \times 10^5$. Open and filled symbols are used to represent data corresponding to the no-control and with-control measurements, respectively.

At TR = 1.0 without control, the stagnation recovery factor is close to unity at small values of h/d (2–2.5) and increases thereafter. This increase in recovery at large h/d is due to an increased mixing of warmer air, as the jet static temperature is initially below the ambient temperature. Further downstream, an increasingly larger amount of warmer air is entrained and the static temperature of the jet increases with the increase in h/d; hence, there is a net heat addition to the jet. Similar observations were made by Goldstein et al. [22] in their study on impinging circular jets. With the microjet control, the stagnation recovery factor remains close to unity over a large extent of h/d (up to 5) and the values are lower compared with the no-control case. Alvi et al. [19], with the help of PIV measurements, showed that microjet control significantly reduces the entrainment of the primary jet flow. Therefore, this reduced entrainment of warmer ambient air into the jet leads to lower temperature recovery with control.

For hot jets (TR = 1.2–1.6), the stagnation recovery factor is close to unity for small h/d values and reduces thereafter. This decrease in the recovery factor at large h/d is once again attributed to a greater mixing of ambient air, which is relatively cooler in the case of hot jets compared with the static temperature in the jet. In this case, as the jet flows downstream, an increasingly larger amount of cold ambient air is entrained and the jet static temperature decreases with increasing h/d. This, in turn, leads to lower total temperatures compared with the initial state. The ambient air close to the jet becomes warmer due to enhanced mixing, and there is a net outflow of heat flux from the jet to the ambient air. The stagnation recovery factor with control at higher temperature ratios is higher than without control, once again emphasizing the reduction of jet entrainment and mixing of the primary jet with the ambient environment when control is on.

C. Hover Lift Loss

The jet-induced negative lift force on the lift plate, known as hover lift loss (Krothapalli et al. [7] and Alvi et al. [15]), has been estimated from the measurements of radially distributed static surface pressures on the lift plate. As mentioned earlier, 19 pressure ports along a radial line were used to obtain the integrated forces. Lift-loss variation as a function of h/d at temperature ratios of TR = 1.0 and 1.4, representative of cold and hot flow conditions, respectively, is shown in Fig. 5. The negative lift force so generated is normalized with the primary jet thrust estimated using isentropic relations.

For cold jets (TR = 1.0, Fig. 5a), the results clearly show that there is a substantial amount of lift loss at small h/d values and more than 50% at $h/d = 1.5$, decreasing monotonically with h/d and becoming nearly negligible beyond $h/d \geq 5$. The activation of microjet control leads to a large reduction in lift loss at small values of h/d.

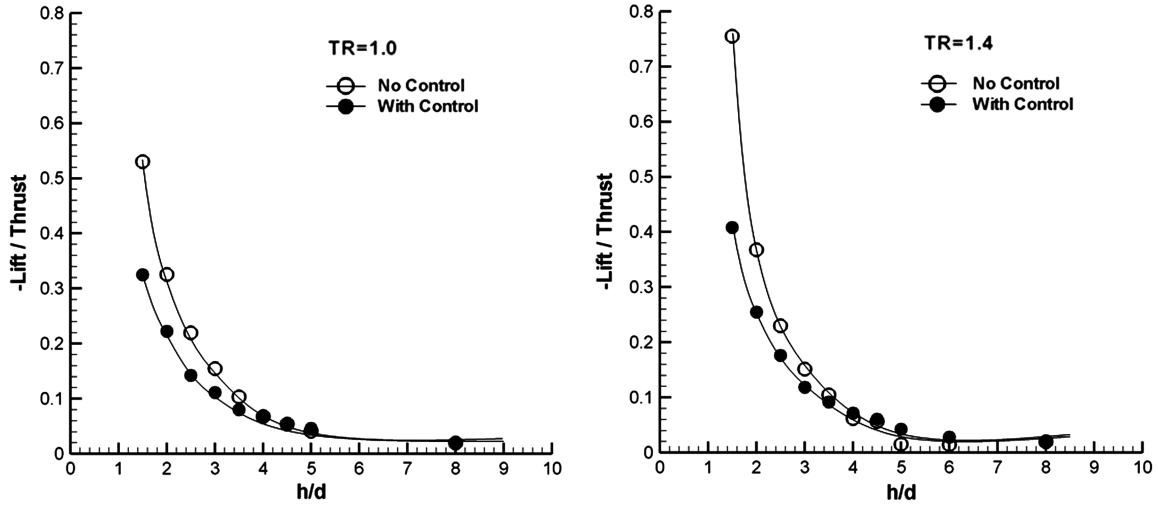

a) TR = 1.0 **b) TR = 1.4**

Fig. 5 Variation of lift loss with nozzle-to-plate distance.

This is particularly important in the context of hover conditions, typically $h/d = 1$–6; for example, at $h/d = 1.5$, the lift loss is reduced by nearly 40% with control. This reduction in lift loss with microjet control is expected because the high entrainment in the jet near field, which leads to the vacuum pressures at the lift plate, is now reduced. These results are very similar to those reported in previous studies (Krothapalli et al. [7] and Alvi et al. [15]).

The variations of lift loss with h/d for hot jets (TR = 1.4) are shown in Fig. 5b. Overall, the lift-loss behavior of the heated jet is similar to that of the cold jet, with a very high lift loss (suck-down forces) at small values of h/d, a monotonous decrease with increasing h/d, and a nearly negligible lift loss for $h/d \geq 5$. However, the magnitude of lift loss for hot jets is significantly higher (up to 75%) as compared with the cold jet (nearly 50%) at $h/d = 1.5$. These higher lift-loss values are alarming because the high-temperature impinging jets such as those occurring in practical conditions induce very high lift loss, particularly at small nozzle-to-plate distances corresponding to the hover conditions. The effect of microjet-based control is very encouraging, with nearly 50% of lift loss is recovered at $h/d = 1.5$.

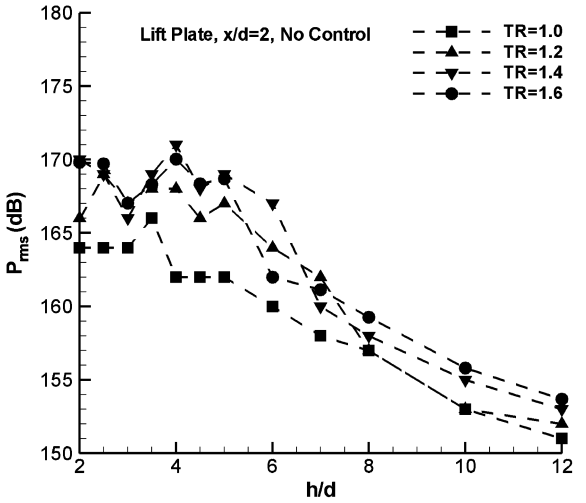

Fig. 7 Effect of temperature ratio on the pressure fluctuation intensities on the lift plate.

D. Unsteady Characteristics of Impinging Jets

1. Unsteady Pressure Field

Unsteady pressure measurements on the lift plate were made at $x/d = 2$ and 3 and on the ground plane at $x/d = 0$ and 2 (all distances are with respect to centerline of the jet) at all four temperature ratios. The intensity of unsteady pressure fluctuations on the lift plate and ground plane as a function of h/d is presented in terms of P_{rms} (expressed in terms of decibels, using a 20 μPa reference). Near-field acoustic measurements were obtained using a microphone located at $x/d = 15$ from the jet centerline and are presented in terms of OASPL in decibels. The pressure fluctuation intensities at TR = 1.0 and 1.4 for the ground plane and lift plate along with the OASPL from the microphone are shown in Figs. 6a and 6b, respectively. At TR = 1.0 (Fig. 6a), the rms pressure levels on the ground plane are the highest, followed by the lift plate and near-field microphone. As observed in previous studies on impinging jets [7,15–19], the magnitude of P_{rms} on the lift plate and OASPL at the near-field microphone is strongly dependent on the nozzle-to-plate distance and is in general high at small h/d ($h/d = 2$–6) and decreases at larger h/d. Overall similar trends in unsteady pressure fluctuations with h/d are observed for the hot jet at TR = 1.4 (pressure fluctuation levels are the highest on the ground plane followed by the lift plate and microphone). However, the magnitudes at TR = 1.4 at comparable h/d are significantly higher at most measurement locations and the variation with h/d is slightly different for the near-field microphone. For example, although the P_{rms} levels for the hot and cold jets are comparable at the impingement point ($x/d = 0$) on the ground plane, the levels are notably higher for the hot jet at $x/d = 2$, which corresponds to the radial wall jet region (Alvi and Iyer [6], Alvi et al. [15]). Similarly, the unsteady pressures for the hot jet are higher on the lift plate at both sensor locations, $x/d = 2$ and 3. The most noticeable increase is in the near-field noise, which is significantly higher for the hot impinging jet compared with the cold jet, by as much as 9 dB in some cases. As expected, these observations indicate that the impinging jet environment becomes harsher as the temperature of the jet increases, both from a structural fatigue and an environmental noise perspective.

The variation of P_{rms} on the lift plate at $x/d = 2$ as a function of h/d at various temperature ratios is shown in Fig. 7. The heated jet shows a significant increase (a maximum of 9 dB at $h/d = 4$) in the overall pressure fluctuation levels as compared with the cold jet. This increase is most notable in going from cold to TR = 1.2 with lower increments at higher TR values, in general. The enhancement in the pressure fluctuations due to an increase in temperature may be due to a number of factors: an increase in jet velocity, a stronger feedback loop, and an enhanced entrainment of ambient fluid into the jet. It may also be observed that, on the lift plate, relatively higher pressure fluctuations persist over a larger extent of h/d ($h/d = 2$–6) for the hot jet compared with the cold jet, suggesting the existence of a stronger feedback loop over a larger extent of h/d at high temperatures. Figure 8 shows the variation of P_{rms} at the stagnation point ($x/d = 0$) on the ground plane as a function of h/d at various

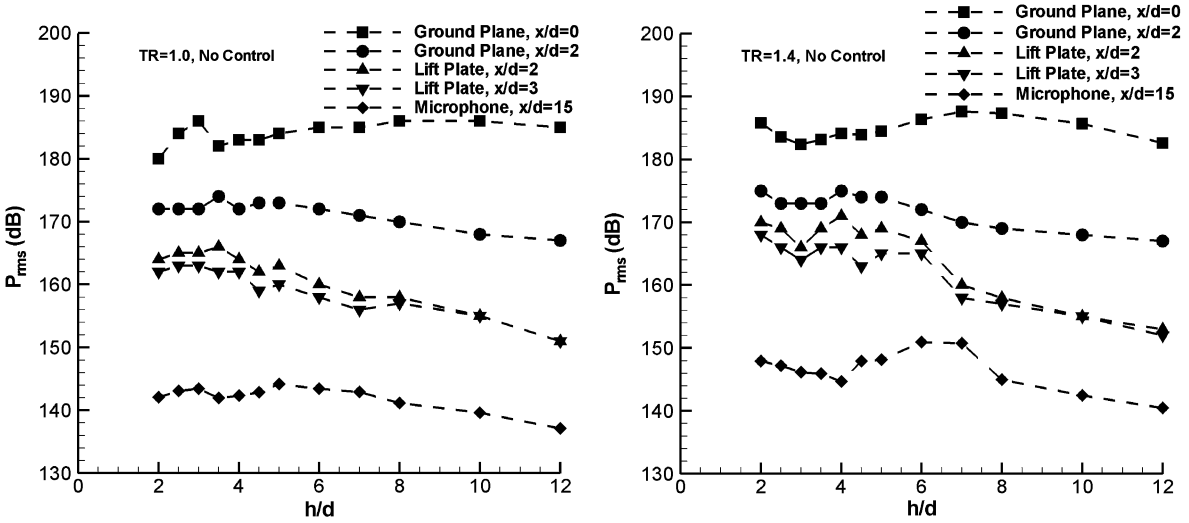

a) TR = 1.0 **b) TR = 1.4**

Fig. 6 Pressure fluctuation intensities at various measurement locations.

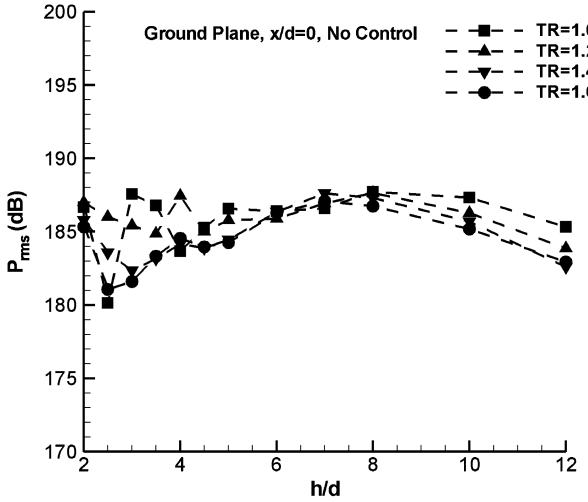

Fig. 8 Effect of temperature ratio on the pressure fluctuation intensities on the ground plane.

temperature ratios. The pressure fluctuations at the stagnation point are relatively unaffected by temperature over the range of TR tested except for small h/d values (≤ 5), at which the pressure fluctuation intensities are higher at lower temperature ratios (TR $= 1.0$ and 1.2). As discussed by Gubanova et al. [23] and Alvi and Iyer [6], this impingement region is dominated by the presence (or absence) of a stagnation bubble and its oscillation. The occurrence of a stagnation bubble is in turn strongly dependent on the shock structure in the mean flowfield in the main jet. Hence, the unsteady loads at the impingement point may be less influenced by the impinging jet feedback loop. However, if one examines ground plane measurements in the wall jet region, for example, at $x/d = 2$ (not shown here), the increase in P_{rms} with jet temperature is seen in a manner similar to the lift plate loads seen in Fig. 7. We note that the unsteady behavior of the stagnation bubble is likely to *also* be influenced by the feedback loop (see Henderson et al. [8]). However, based on the trends observed in the stagnation region (Fig. 8) and the dependence of the bubble on the mean flowfield, we suggest that it may be less directly influenced by the feedback loop and more by the mean flowfield. Nevertheless, it is difficult to separate these two effects and this issue remains unclear.

The effectiveness of microjet control is evaluated in terms of a reduction in the pressure fluctuations, ΔP_{rms}, where $\Delta P_{\text{rms}} = P_{\text{rms (no control)}} - P_{\text{rms (with control)}}$. This is shown in Fig. 9 for the lift plate sensors at various temperature ratios and as a function of h/d. This figure clearly shows that the fluctuating loads on the lift plate are significantly reduced with the activation of microjets at all temperature ratios. In fact, the reduction in P_{rms} is significantly higher (up to 15 dB) at higher temperature ratios. Also, the effectiveness of control at high temperatures is significant over a larger extent of nozzle-to-plate distances. Figure 10 shows the reduction in P_{rms} at the stagnation point on the ground plane at four temperature ratios. As discussed earlier, because the impingement region may be dominated by the stagnation bubble/structure, the reduction in P_{rms} with increasing temperature does not follow a trend similar to that observed for the lift plate (Fig. 9). However, the results in Fig. 10 show that the pressure fluctuations are once again substantially reduced at all the temperatures tested, with a maximum reduction of 20 dB at TR $= 1.0$ and 1.2. These results further substantiate the fact that microjet-based control is very effective in reducing unsteady loads on the ground surface and nearby (aircraft) structure due to jet impingement.

Similar to the results of microjet control on the lift plate and ground plane, the effectiveness of control on near-field noise in terms of $\Delta\text{OASPL}(=\text{OASPL}_{\text{no control}} - \text{OASPL}_{\text{with control}})$ is shown in Fig. 11. The effect of microjet control in reducing the near-field noise is clearly evident, and the effectiveness is nearly the same at all temperature ratios over the range of h/d tested.

The narrowband pressure spectra for the unsteady pressures at the lift plate, ground plane, and near-field microphone at TR $= 1.0$ at $h/d = 3.0$ are shown in Fig. 12. These spectra clearly show multiple discrete high-amplitude impingement tones associated with the flow-acoustic resonance. Moreover, these tones are at identical

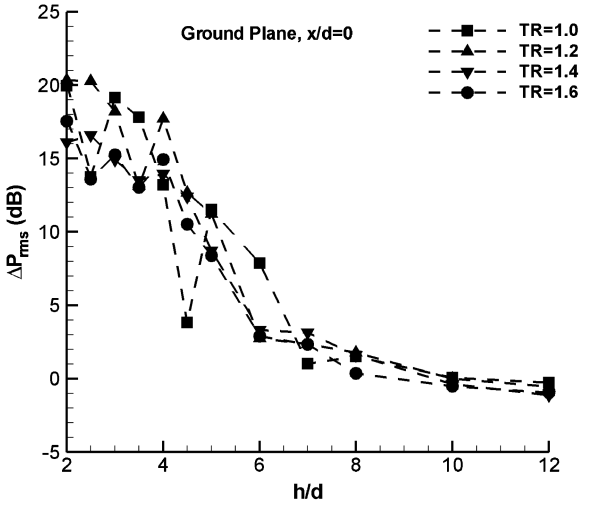

Fig. 10 Reduction in pressure fluctuation intensities at a stagnation point on the ground plane.

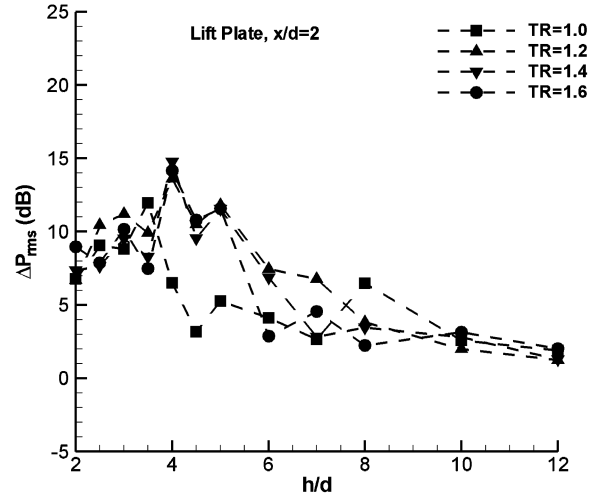

Fig. 9 Reduction in pressure fluctuation intensities on the lift plate.

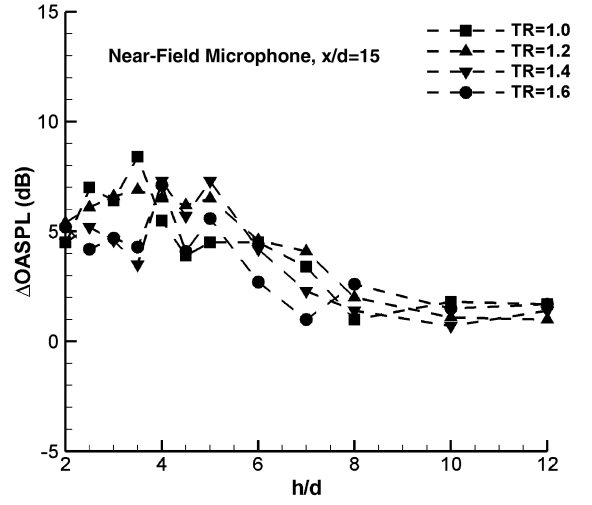

Fig. 11 Reduction in near-field noise levels.

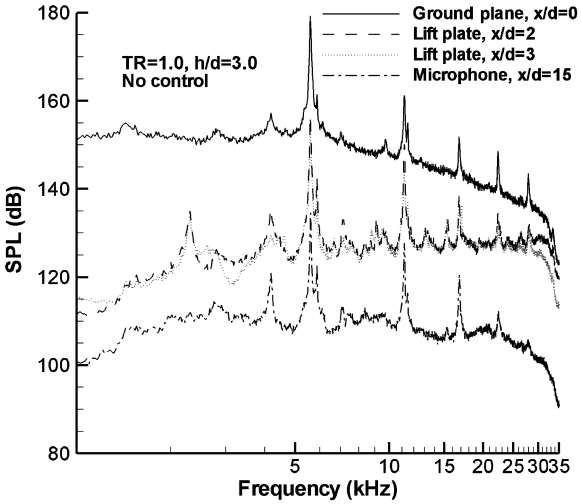

Fig. 12 Narrowband frequency spectra of unsteady pressures and near-field noise at TR = 1.0.

frequencies for all three pressure transducers and the microphone, again confirming the global nature of this resonance/feedback phenomenon. These features of the pressure spectra suggest that any control technique that efficiently attenuates the feedback loop should be able to significantly reduce the unsteady loads (due to unsteady pressures) associated with impinging jets.

The impingement tones on the lift plate are compared with the frequency f_n predicted using Eq. (3) as proposed by Powell [9]. As seen in Fig. 13, there is very good agreement of present results with Powell's predictions.

$$\frac{n+p}{f_n} = \int_0^h \frac{\mathrm{d}h}{C_i} + \frac{h}{C_a} \quad (\text{where } n = 1, 2, 3, \ldots) \tag{3}$$

In Eq. (3), h is the nozzle-to-ground-plane distance, C_i is the convection velocity of the large structures traveling downstream, C_a is the speed of acoustic waves traveling upstream in the ambient environment, n represents different frequency modes, and the phase lag p is chosen or determined from the jet conditions. In the present case, the convection velocity C_i was chosen as $0.5U_j$ (where U_j is the fully expanded jet velocity) and the phase lag was $p = -0.4$. Please note that the value of phase lag p chosen here is not based on any rigorous analysis but is a value that appears to provide a good agreement with the predictions and has been used in previous experiments under similar conditions. More details can be found in Krothapalli et al. [7]. The results clearly show the well-known staging behavior in accordance with the feedback mechanism associated with the impinging jet flowfield, similar to those observed earlier for cold jets [7].

The effect of temperature on the unsteady pressure spectra on the lift plate at $x/d = 2$ and $h/d = 4.0$ is shown in Fig. 14. Note that the tonal frequencies are strongly dependent on the jet temperature, for which an increase in the temperature ratio from 1.0 to 1.4 results in an increase in the tone frequency. Moreover, the amplitude of the primary tone also increases with an increase in the temperature ratio. However, the change in broadband levels with the temperature ratio is less significant.

A comparison of the unsteady pressure spectra on the lift plate and for the near-field noise at TR = 1.4 with and without microjet control is shown in Fig. 15. In both figures the dominant tones associated with the feedback loop are significantly reduced, and some are even eliminated with the activation of control (see Fig. 15b). This again clearly demonstrates the effectiveness of microjet-based active control in disrupting the feedback loop and reducing the associated unsteadiness for heated jets. In addition to a reduction in tones, broadband levels have also been considerably reduced with the activation of control.

2. *Unsteady Temperature Field*

To study the unsteady thermal loading characteristics on the ground plane, we measured the unsteady temperature on the ground plane by scanning the thermocouple signals at 70 kHz. The results are presented in the form of temperature power spectral density in Fig. 16. The figure shows the temperature spectra at TR = 1.0 and 1.4, respectively, at a fixed value of $h/d = 4$. It also includes the effect of control on the unsteady thermal loading. The temperature spectra show high-amplitude, discrete temperature peaks similar to the tones observed in the pressure and noise spectra. Moreover, the frequencies of these thermal peaks are the same as the pressure and acoustic tones observed in the ground plane pressure and near-field microphone measurements (see Fig. 15). The effectiveness of microjet control is clearly seen for both cold and heated jets in terms of the reduction in high-amplitude thermal peaks and broadband temperatures. These results are very encouraging and seem to provide a promising solution for the ground erosion problem associated with hot impinging jets.

E. Particle Image Velocimetry

Global information regarding the evolution of the jet flowfield and the velocity field was obtained using PIV. PIV measurements were

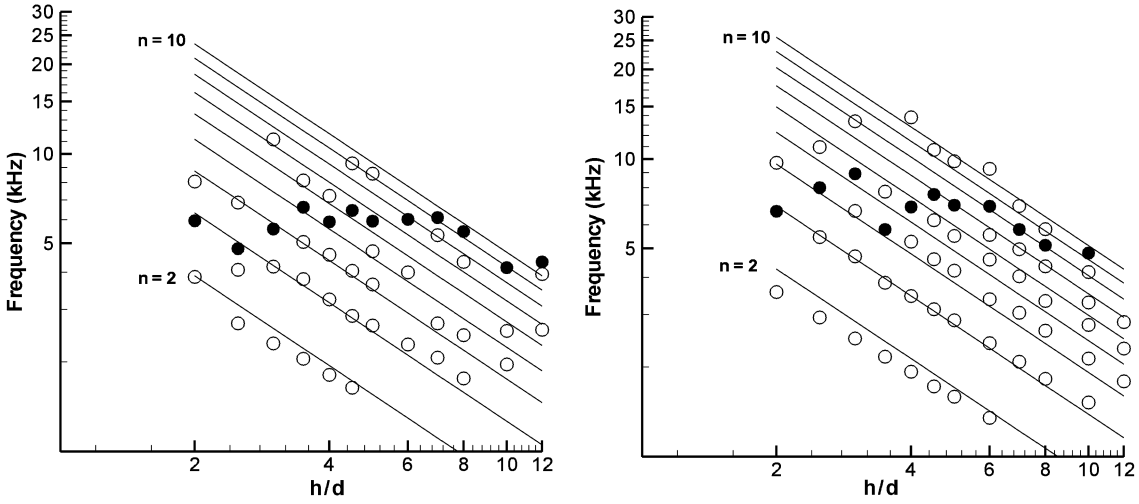

Fig. 13 Comparison of impinging tones represented by symbols with Powell's prediction represented by solid lines; filled symbols represent amplitude dominant tones.

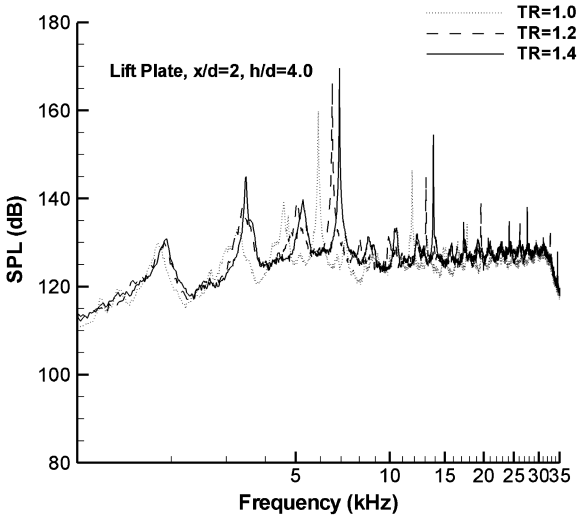

Fig. 14 Effect of temperature ratio on narrowband frequency spectra.

obtained along a streamwise central plane at selected h/d for impinging jets at TR = 1.0 and 1.4, representing cold and hot conditions, respectively. The results are presented in the form of contour plots of the ensemble-averaged (mean) velocity (V_{mean}). Velocity vectors at selected locations are shown superposed on the mean velocity contour plots.

1. *Effect of Temperature*

The contour plots of the mean velocity field corresponding to $h/d = 5$ at TR = 1.0 and 1.4 are shown in Fig. 17. As mentioned earlier, measurements were conducted at NPR = 3.7, corresponding to ideally expanded jet conditions. The length of the vector represents the magnitude of velocity at each location. The velocity vectors at the nozzle exit show that, for both cold and hot jets, the jet exhibits a near top-hat velocity profile (more evident in Fig. 18). At TR = 1.0 (Fig. 17a), the mean jet velocity at the exit plane is ≈430 m/s, corresponding to the fully expanded jet velocity at $M = 1.5$; at TR = 1.4 (Fig. 17b), the velocity at exit is ≈530 m/s, corresponding to a fully expanded jet at $T_0 \approx 420$ K. Because of this difference in velocity range, the maps/contours in Fig. 17 are different. Although the contour plots provide global information, a closer look is required for a better understanding of the effect of temperature. In Fig. 18, we show mean velocity profiles extracted from these contour plots at two streamwise locations, $y/d = 0.5$ and 4.0. At $y/d = 0.5$ (Fig. 18a), a location close to the nozzle exit, we still see the evidence of a top-hat velocity profile; at the downstream location $y/d = 4$, the velocity profiles show a central peak. As expected, the mean velocity for the hot jet is relatively higher than that for the cold jet at both streamwise locations. In Fig. 19, the streamwise mean velocity, when normalized

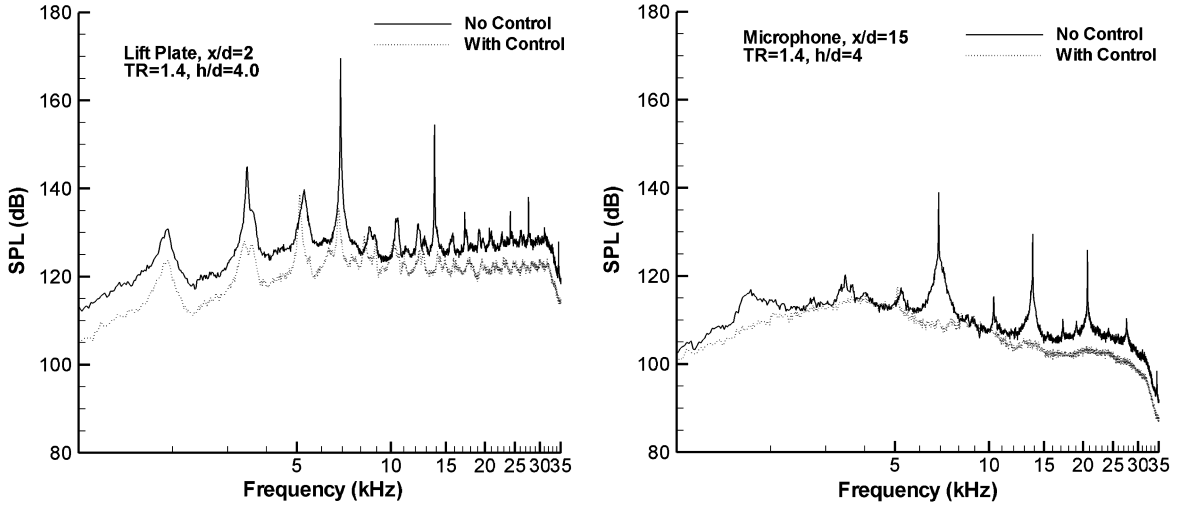

a) Lift plate **b) Microphone**

Fig. 15 Effect of control on narrowband pressure spectra at TR = 1.4 and $h/d = 4$.

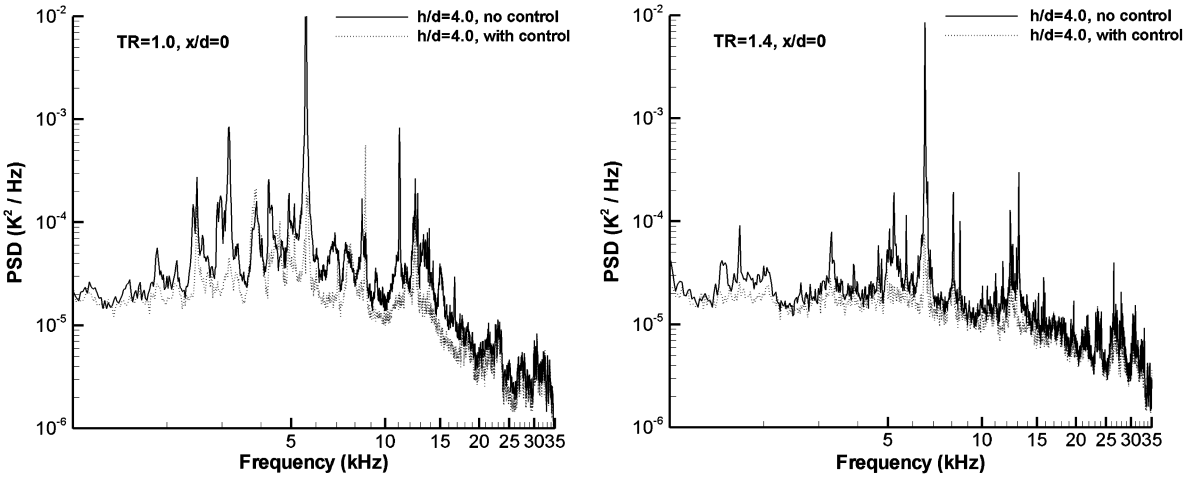

a) Ground plane, TR = 1.0 **b) Ground plane, TR = 1.4**

Fig. 16 Effect of control on narrowband temperature spectra on the ground plane at $x/d = 0$ and $h/d = 4$.

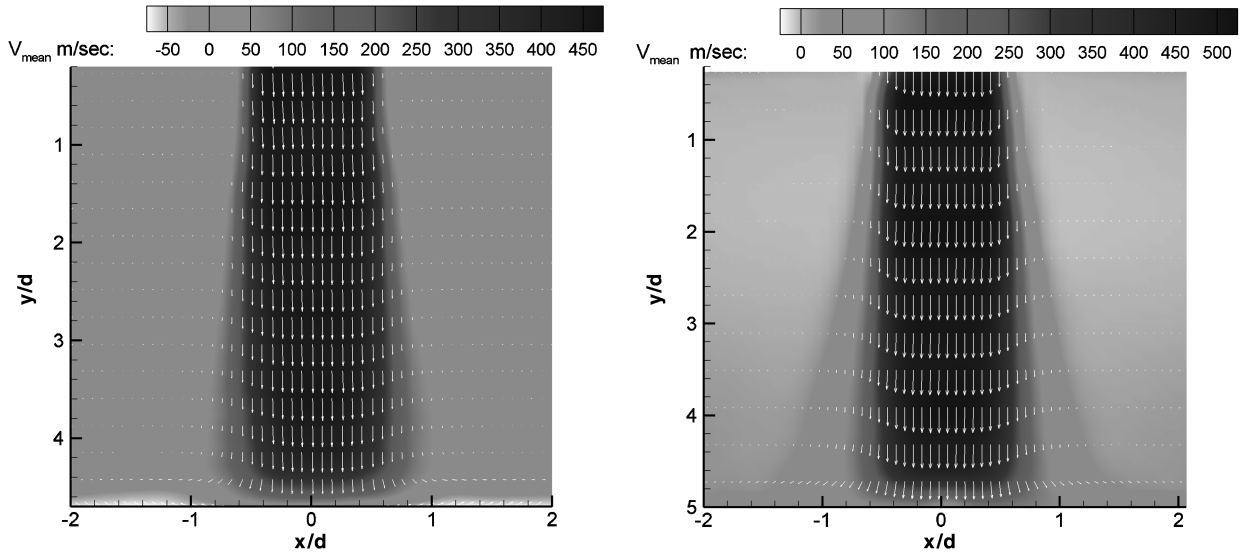

a) TR = 1.0 b) TR = 1.4

Fig. 17 Mean velocity distributions in the central plane of the impinging jet at $h/d = 5$ and no control (note that the contour levels for the hot and cold jets are different).

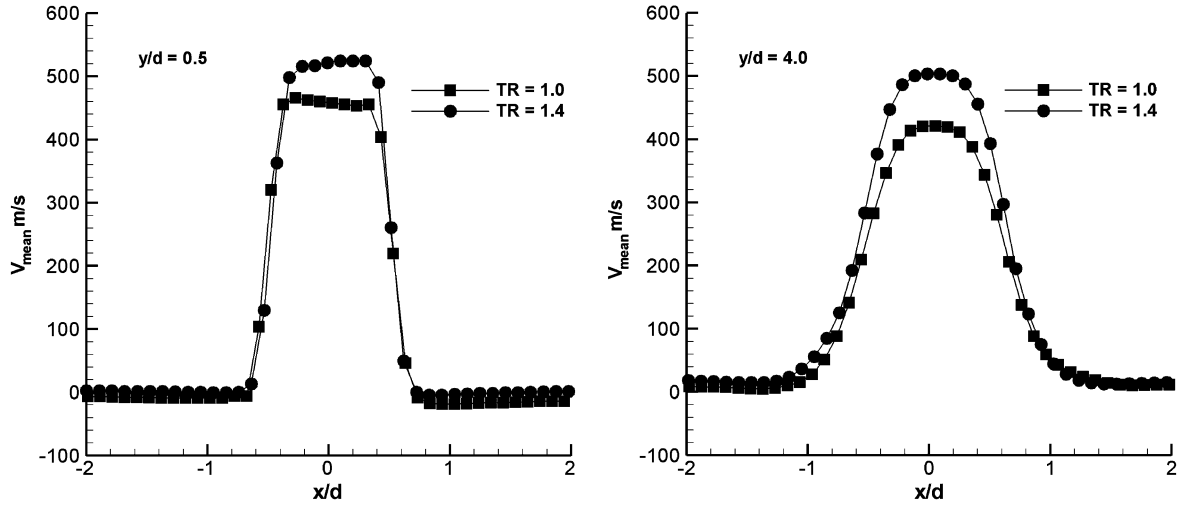

a) At y/d = 0.5, no control b) At y/d = 4.0, no control

Fig. 18 Mean velocity distribution for the hot and cold jets at two locations without control.

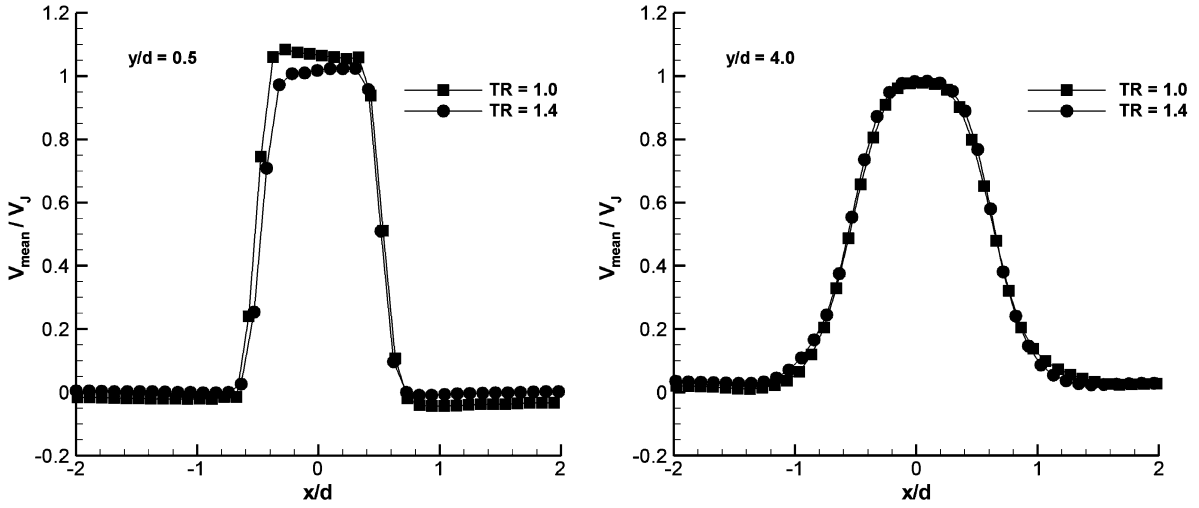

a) At y/d = 0.5, no control b) At y/d = 4.0, no control

Fig. 19 Normalized mean velocity distribution for hot and cold jets at two locations without control.

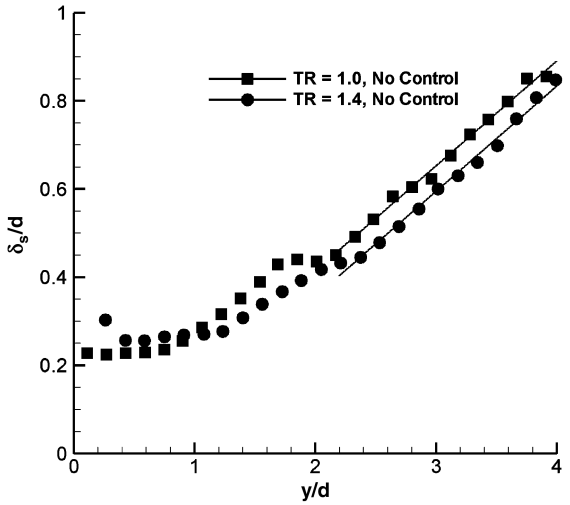

Fig. 20 Effect of temperature on the growth of shear-layer thickness.

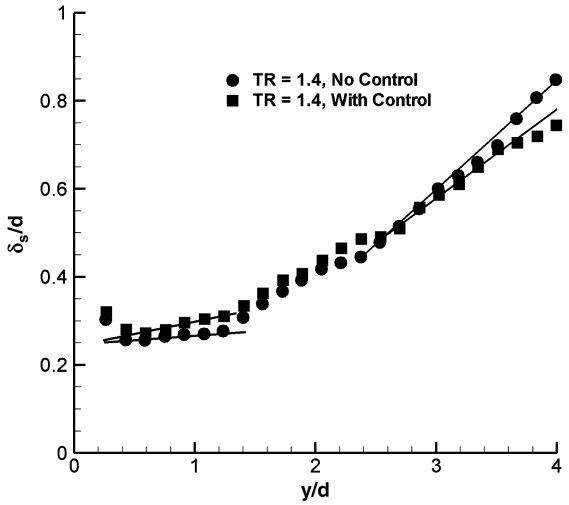

Fig. 22 Effect of temperature on the growth of shear-layer thickness.

using the fully expanded jet velocity V_J, shows an excellent collapse at the downstream location ($y/d = 4$, Fig. 19b), whereas some differences at $y/d = 0.5$ (Fig. 19a) are observed, especially in the jet shear layer. Although not shown here, the entrainment velocities near the exit plane for the hot jet (TR = 1.4) are also higher, resulting in a larger amount of suction at the lift plate for hot jets as compared with the cold jets. This results in a higher lift loss for hot impinging jets, as observed earlier in Fig. 5.

To further quantify the effect of temperature on shear-layer characteristics, the shear-layer thickness was extracted from the velocity field for both the cold and hot jets. The shear-layer thickness δ_S is defined as $\delta_S = r_{0.95} - r_{0.05}$, where $r_{0.95}$ and $r_{0.05}$ are the radial locations where the mean velocities are 95% and 5% of the local jet centerline velocity, respectively. The growth of the shear layer with streamwise distance y/d is shown in Fig. 20. In the initial region ($y/d < 1$), close to the nozzle exit, the hot-jet shear layer is measurably thicker than that for the cold jet, whereas in the region $1 < y/d < 2$, the cold jet appears to spread more than the hot jet. In the initial region, the spreading rate is nonlinear, but it becomes linear beyond $y/d > 2$ for both the cold and hot jets. The growth rate in the linear region is shown by the solid lines.

2. *Effect of Microjet Control*

The effect of microjet control on the mean velocity distributions of the impinging jet at TR = 1.0 and 1.4 is shown in Fig. 21. In general, the velocity flowfield with (Fig. 21) and without (Fig. 17) control are globally similar and show nearly the same flow features. These results suggest that most of the mean flow properties of the jet remain unaltered with control. However, a closer look at the shear-layer growth for the hot jet (TR = 1.4) with and without control (Fig. 22) reveals some differences. The first noteworthy difference is that, near the jet exit ($y/d \leq 1$), the hot jet without control appears to spread at a lesser rate (indicated by a lower slope) than that with control near the nozzle exit. However, further downstream ($y/d > 2$), the jet without control spreads at a higher rate (higher slope) than the jet with control. These results are similar to those observed in previous studies on cold impinging jets [16–19], except that the crossover for the cold jet was at $y/d = 1$. As discussed in previous studies, this initial thickening of the shear layer with control will reduce the receptivity of the shear layer and weaken the feedback loop, which in turn stabilizes the flow and reduces unsteady loads, as already noted in Sec. III.D (Figs. 9–11).

IV. Conclusions

The flow and acoustic field created by high-temperature supersonic impinging jets, such as those occurring in STOVL aircraft, are highly complex. There have been many attempts in the past to understand this highly oscillatory flowfield and the associated feedback loop responsible for the adverse performance-related

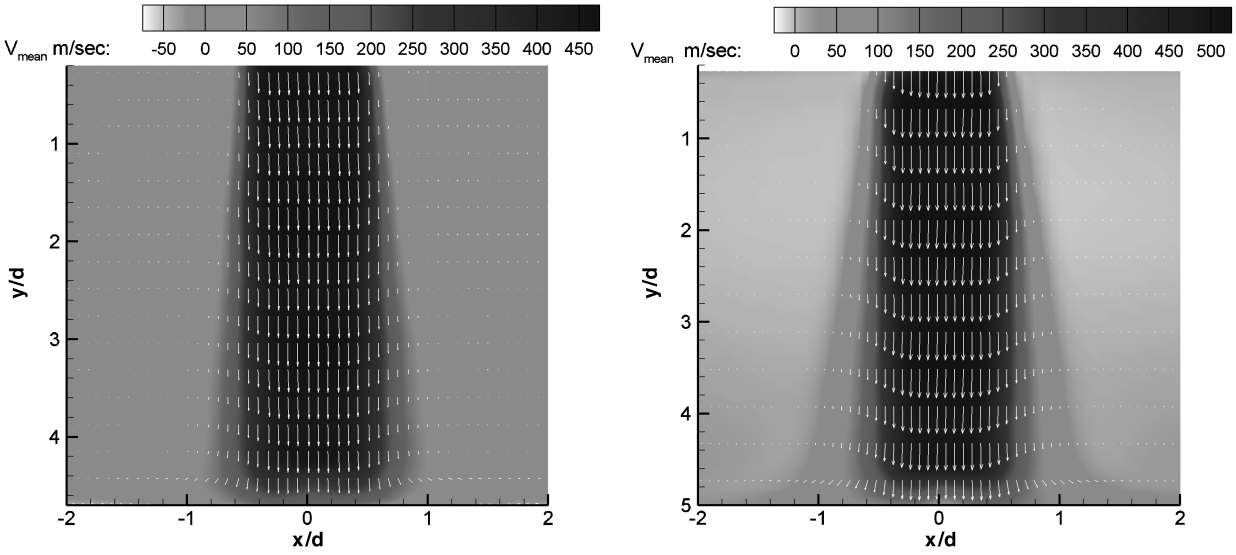

a) TR = 1.0 b) TR = 1.4

Fig. 21 Mean velocity distributions with microjet control.

effects. The present study is an attempt to characterize hot impinging jets, primarily to study the effect of temperature on flowfield characteristics and the associated feedback loop. We also aimed to examine the effectiveness of microjet control for a heated impinging jet over a range of temperature ratios.

The experimental results described in this paper are temperature distributions on the ground plane, lift-loss characteristics, unsteady pressures on the lift plate and ground plane, and acoustic measurements in the near field. The velocity field for both the cold and hot conditions and a few typical flow visualization images are also presented to show the overall features of the jet flowfield. The results show that the stagnation temperature recovery factor strongly depends on the temperature ratio and the nozzle-to-plate distance. The mixing characteristics play an important role in the variation of the stagnation recovery factor and, in turn, on the heat transfer characteristics at the impingement plane. The jet-induced lift loss at higher temperatures is significantly higher than that for the cold jet at the same Mach number. Equally important and encouraging is the outcome that microjet control provides a substantial recovery of lift loss (nearly 50%) at higher temperatures.

The unsteady pressure fluctuations associated with high-tempeature impinging jets are significantly higher than those for cold jets. The activation of microjets leads to dramatic reductions in the rms pressure fluctuations on the ground plane (up to 20 dB) and the lift plate (up to 15 dB), as well as in the near-field sound pressure levels (up to 8 dB). Microjet control not only attenuated or sometimes even eliminated the discrete high-amplitude impinging tones, but also reduced the broadband noise levels considerably. The temperature spectra showed high-temperature peaks at the same frequencies as the impingement tones in the pressure spectra, indicating unsteady thermal loading and a major cause of ground erosion. These temperature peaks and associated broadband temperatures were also significantly reduced with microjet control. Velocity field measurement results show that the entrainment velocities near the exit plane for the hot impinging jet are much higher than for the cold impinging jet, resulting in much higher lift loss, consistent with the static pressure measurements. In summary, this study shows that the feedback loop and the adverse effects associated with impinging jets become more dominant as the jet temperature is increased (at least over the range examined). At the same time, microjet control continues to be very effective in controlling this oscillatory flowfield.

Acknowledgments

This research was in part supported by a grant from the U.S. Air Force Office of Scientific Research, monitored by R. Jefferies and J. Schmisseur. We are grateful for this support. The authors would also like to thank the staff of AAPL, especially I. Choutapalli and R. Avant, for their help with these experiments. We would also like to acknowledge the Florida Center for Advanced Aero-Propulsion for supporting part of this research.

References

[1] Donaldson, C. D., and Snedeker, R. S., "A Study of Free Jet Impingement. Part 1. Mean Properties of Free And Impinging Jets," *Journal of Fluid Mechanics*, Vol. 45, No. 2, 1971, pp. 281–319. doi:10.1017/S0022112071000053

[2] Lamont, P. J., and Hunt, B. L., "The Impingement of Underexpanded Axisymmetric Jets on Perpendicular and Inclined Flat Plates," *Journal of Fluid Mechanics*, Vol. 100, 1980, pp. 471–511. doi:10.1017/S0022112080001255

[3] Powell, A., "The Sound-Producing Oscillations of Round Underexpanded Jets Impinging on Normal Plates," *Journal of the Acoustical Society of America*, Vol. 83, 1988, pp. 515–533. doi:10.1121/1.396146

[4] Tam, C. K. W., and Ahuja, K. K., "Theoretical Model of Discrete Tone Generation by Impinging Jets," *Journal of Fluid Mechanics*, Vol. 214, 1990, pp. 67–87. doi:10.1017/S0022112090000052

[5] Messersmith, N. L., "Aeroacoustics of Supersonic and Impinging Jets," AIAA Paper 1995-0509, 1995.

[6] Alvi, F. S., and Iyer, K. G., "Mean and Unsteady Flow Field Properties of Supersonic Impinging Jets with Lift Plates," AIAA Paper 1999-1829, 1999.

[7] Krothapalli, A., Rajkuperan, E., Alvi, F. S., and Lourenco, L., "Flow Field and Noise Characteristics of a Supersonic Impinging Jet," *Journal of Fluid Mechanics*, Vol. 392, 1999, pp. 155–181. doi:10.1017/S0022112099005406

[8] Henderson, B., Bridges, J., and Wernet, M., "An Experimental Study of the Oscillatory Flow Structure of Tone Producing Supersonic Impinging Jets," *Journal of Fluid Mechanics*, Vol. 542, 2005, pp. 115–137. doi:10.1017/S0022112005006385

[9] Powell, A., "On Edge Tones and Associated Phenomena," *Acustica*, Vol. 3, 1953, pp. 233–243.

[10] Karamcheti, K., Bauer, A. B., Shields, W. L., Stegen, G. R., and Woolley, J. P., "Some Features of an Edge Tone Flow Field," NASA SP 207, 1969, pp. 275–304.

[11] Kweon, Y.-H., Miyazato, Y., Aoki, T., Kim, H.-D., and Setoguchi, T., "Control of Supersonic Jet Noise Using a Wire Device," *Journal of Sound and Vibration*, Vol. 297, 2006, pp. 167–182. doi:10.1016/j.jsv.2006.03.033

[12] Elavarasan, R., Krothapalli, A., Venkatakrishnan, L., and Lourenco, L., "Suppression of Self-Sustained Oscillations in a Supersonic Impinging Jet," *AIAA Journal*, Vol. 39, No. 12, 2001, pp. 2366–2373. doi:10.2514/2.1243

[13] Sheplak, M., and Spina, E. F., "Control of High Speed Impinging-Jet Resonance," *AIAA Journal*, Vol. 32, No. 8, 1994, pp. 1583–1588. doi:10.2514/3.12147

[14] Shih, C., Alvi, F. S., and Washington, D., "Effects of Counterflow on the Aeroacoustic Properties of a Supersonic Jet," *Journal of Aircraft*, Vol. 36, No. 2, 1999, pp. 451–457. doi:10.2514/2.2451

[15] Alvi, F. S., Shih, C., Elavarasan, R., Garg, G., and Krothapalli, A., "Control of Supersonic Impinging Jet Flows Using Supersonic Microjets," *AIAA Journal*, Vol. 41, No. 7, 2003, pp. 1347–1355. doi:10.2514/2.2080

[16] Lou, H., Shih, C., and Alvi, F. S., "A PIV Study of Supersonic Impinging Jet," AIAA Paper 2003-3263, 2003.

[17] Lou, H., Alvi, F. S., and Shih, C., "Active and Adaptive Control of Supersonic Impinging Jets," *AIAA Journal*, Vol. 44, No. 1, 2006, pp. 58–66. doi:10.2514/1.13347

[18] Kumar, R., Lazic, S., and Alvi, F. S., "Active Control of High Temperature Supersonic Impinging Jets," AIAA Paper 2008-360, 2008.

[19] Alvi, F. S., Lou, H., Shih, C., and Kumar, R., "Experimental Study of Physical Mechanisms in the Control of Supersonic Impinging Jets Using Microjets," *Journal of Fluid Mechanics*, Vol. 613, 2008, pp. 55–83.

[20] Alkislar, M. B., Krothapalli, A., and Butler, G. W., "The Effect of Streamwise Vortices on the Aeroacoustics of a Mach 0.9 Jet," *Journal of Fluid Mechanics*, Vol. 578, 2007, pp. 139–169. doi:10.1017/S0022112007005022

[21] Lourenco, L. M., and Krothapalli, A., "True Resolution PIV: A Mesh-Free Second Order Accurate Algorithm," *Proceedings of 10th International Symposium on Applications of laser Techniques in Fluid Mechanics*, Springer–Verlag, Berlin/New York/Heidelberg, 2000.

[22] Goldstein, R. J., Behbahani, A. I., and Heppelmann, K. K., "Streamwise Distribution of the Recovery Factor and the Local Heat Transfer Coefficient to an Impinging Circular Air Jet," *International Journal of Heat and Mass Transfer*, Vol. 29, No. 8, 1986, pp. 1227–1235. doi:10.1016/0017-9310(86)90155-9

[23] Gubanova, O. I., Lunev, V. V., and Plastinina, L. N., "The Central Breakaway Zone with Interaction Between a Supersonic Underexpanded Jet and a Barrier," *Fluid Dynamics*, Vol. 6, 1973, pp. 298–301. doi:10.1007/BF01015070

N. Chokani
Associate Editor